Cracking of Nanofilm-based Devices for Electrochemical Energetics

Benedetto Bozzini[1], Marco Boniardi[2], Alessandra Gianoncelli[3], Burkhard Kaulich[4], Claudio Mele[1], Mauro Prasciolu[5], Gennaro Scarselli[1] and Maya Kiskinova[3]

[1] Dipartimento di Ingegneria dell'Innovazione, Università del Salento, via per Arnesano, I-73100 Lecce, Italy; benedetto.bozzini@unisalento.it
[2] Dipartimento di Meccanica, Politecnico di Milano, via La Masa 34, I-20156 Milano, Italy; marco.boniardi@polimi.it
[3] Elettra-Sinctrotrone Trieste SCpA, S.S. 14, km 163.5 in Area Science Park 34149 Basovizza (TS), Italy; maya.kiskinova@elettra.trieste.it
[4] Diamond Light Source, Harwell Science and Innovation Campus, Didcot, OX11 0DE, UK; burkhard.kaulich@diamond.ac.uk
[5] Desy, D-22607 Hamburg – D; mauro.prasciolu@desy.de

ABSTRACT. *Fabrication and testing of fuel-cells based on nanofilm electrodes and interconnects is a hot technological challenge for three key reasons: (i) miniaturisation and integration into electronic devices as well as implementation of on-chip logics, (ii) testing of the performance of nano-materials on their real scale and (iii) use of cutting-edge material characterisation techniques. The principal interest of a nanotechnological approach to material problems in electrochemical energetics is particularly related to long-term durability issues of critically degradable components. Among the degradation modes, mechanical failure by cracking of the functional thin films is being recognised as a crucial one, impairing the implementation of laboratory systems into real-life devices. In this paper we report on corrosion-induced local thinning and correlated cracking of electrode components in a RTIL-based Proton Exchange Membrane Fuel Cell with Pt micro-particles as catalyst, Au feeder electrodes and Fe interconnects. In situ imaging of the multi-material system in electrochemical environment, based on X-ray scanning and optical microscopies, has disclosed the formation of complex cracking patterns, including spiral cracks. A simple mechanical explanation of the peculiar cracking pattern is proposed.*

INTRODUCTION

The background to this study is the implementation of metallic nanofilms in polymer electrolyte nano-fuel cells [1-6]. This paper reports a study based on soft X-ray transmission (STXM) and optical microscopy (OM), in conjunction with simple mechanical modelling of peculiar cracking modes correlated with the corrosion of Fe nanofilms in contact with 1-butyl-1-methyl-pyrrolidinium bis (trifluoromethylsulfonyl)

amide ([BMP][TFSA]) room-temperature ionic liquid (RTIL). Fabrication of nano fuel-cells is a serious technological challenge for miniaturisation and integration into electronic devices and implementation of on-chip systems. The principal interest of fuel-cell material problems is particularly related to durability issues of critically degradable Proton Exchange Membrane Fuel Cell (PEMFC) components, such as: membranes, catalysts and interconnects (e.g. [7, 8]). The ideal service-life without major maintenance actions for a PEMFC should amount to several tens of thousands hours, a target performance currently far from achievement. A nanotechnology approach is the key to attain a long-term material performance since an anticorrelation has been conjectured between the spatial scale of controlled defects in a given material and the timescale of the material durability [9]. In the special case of PEMFCs, nanotechnologies can offer improved routes to the fabrication of several components as detailed in [2]. As far as interconnect materials are concerned, bipolar materials using nanocomposites have been considered in order to achieve higher durability and lower contact resistance between bipolar plates and gas-diffusion layers [10]. Composite CNT/PTFE films, exhibiting a typical electrical conductivity of ca. 10 S cm^{-1}, have been used to coat 304 stainless-steel.

In the quest towards FC nanofabrication, some of the authors have developed devices for in situ scanning STXM, a very promising method for shedding light on the response of nano-components of FCs to the electrochemical operating conditions prevailing in a given zone of the device. The feasibility of in situ electrochemical experiments with this approach has been demonstrated by a series of works performed by our group at the TwinMic beamline of the Elettra Synchrotron, extending the idea in order to improve the cell configuration and to allow the investigation of a range of faradaic processes [3-6].

This paper is focussed on peculiar mechanico-electrochemical failure modes of the Fe interconnects of cells implementing a composite Nafion/RTIL electrolyte, Pt black as catalyst, an Au feeder electrode and an Fe test electrode. Cathodic conditions were simulated by dosing O_2 in the vacuum of the microscope, bringing the background pressure to 2.5×10^{-5} mbar: O_2 pressures of this entity and even one order of magnitude lower have been proved to be enough to ensure the possibility of running faradaic electrochemistry [11]. Anodic conditions were achieved by using $NaBH_4$ as a non-hydrogen base fuel for PEMFC [12], dissolved in the RTIL component of the composite electrolyte.

MATERIALS AND METHODS

Cell fabrication and operating conditions

The electrochemical cell was fabricated along the lines detailed in [4]. In this version of the thin-layer cell for STXM work, we have introduced a spun composite electrolyte that is stable in vacuo and can thus be used without need of sealing the electrochemical

cell. Figure 1 illustrates schematically the layout of the cell fabricated on an X-ray transparent Si_3N_4 window. The supported electrode assembly, consisting of two square, 40 nm thick Au and 75 nm thick Fe electrodes deposited by evaporation. On top, a 200 nm thick composite electrolyte, containing the Pt black catalyst, is applied by spinning, covering all the window so that the central cross-shaped region consist only of electrolyte. The computed primary current density distribution is also shown in Figure 1. Au and Fe were chosen as feeder electrode materials for the following reasons. Au simulates the electrochemical behaviour of inert contact materials (typically, the combination of the gas-diffusion layer and interconnect). Fe provides information on steel-based bipolar-plates, yielding the well-known corrosion problems ([4, 13] and references therein contained). These half-cells can be electrochemically polarised in several ways, representative or technologically relevant situations: (i) by applying the proper polarisation to the Au electrode and imaging it, one simulates fuel-cell performance with ideally stable contact materials; (ii) with a similar procedure applied to the Fe electrode, one simuates fuel-cell performance with steel-based metallic bipolar plates; (iii) by shorting the Au and Fe electrodes, one simulates the standby conditions of a fuel-cell with steel-based bipolar plates; this type of electrochemical polarisation has been successfully employed in similar work in aqueous and RTIL environments [3, 4]. The composite electrolyte was prepared by mixing 1g of 1-butyl-1-methyl-pyrrolidinium bis (trifluoromethylsulfonyl) amide ([BMP][TFSA]), purchased from IoLiTec with 8 mL of Aldrich 274704 - 5 wt. % Nafion solution in lower aliphatic alcohols/H_2O mix. To this mixture, 2 mg of Aldrich 205915 – Pt black were added. For the preparation of the anodic cells, the fuel was added to the electrolyte by saturating [BMP][TFSA] with $NaBH_4$ powder (Aldrich 16940-66-2) before mixing it with the Nafion solution. The resulting systems were subjected to unltasonic agitation for 1 hour before application to the cells. The electrolyte-catalyst or electrolyte-catalyst-fuel mixtures were deposited by spin coating technique onto the lithographed cells. A layer thickness of 200 nm was achieved by using 4000 rpm spinning rate. For the operation of the anodic half-cell, the background pressure of the TwinMic analysis chamber (10^{-6} mbar), was kept throughout the experiments. Cathodic conditions were simulated by dosing ultra high-purity O_2 (Sapio), reaching 2.6×10^{-5} mbar.

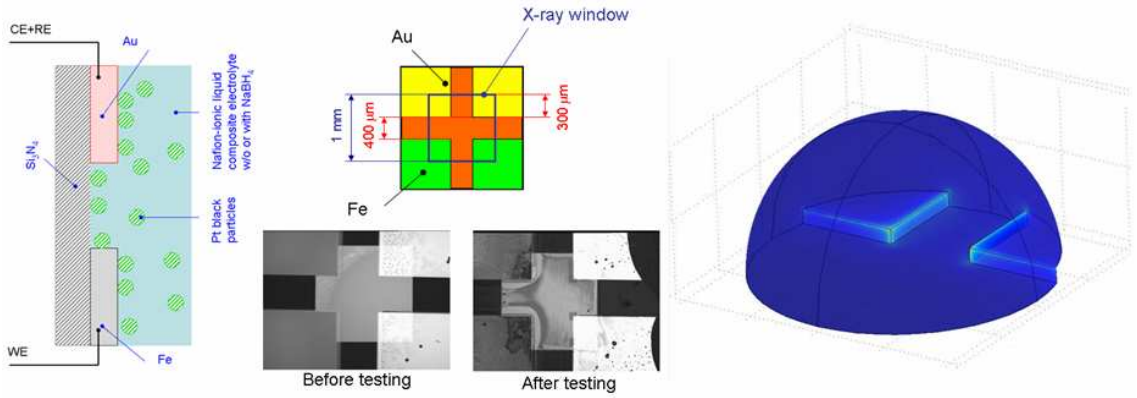

Figure 1 - Nano-FC concept, layout and micrographs of cell in pristine conditions and after testing. Right graph shows primary current density distribution (arbitrary units).

The soft X-ray imaging analyses were carried out using the TwinMic instrument at Elettra synchrotron facility, which works in the soft energy range (400-2200 eV). The X-ray beam is focused onto the specimen through a zone plate diffractive optics, able to provide sub-100 nm spatial resolution [1]. The present experiments were carried out with photon energy at 740 eV, i.e. above the varying across the Fe L absorption edge, enhancing the contrast of Fe features.

RESULTS AND DISCUSSION

Electrochemical testing and in situ imaging

In view of testing the electrochemical behaviour of the nano-FCs, potentiostatic measurements corresponding to "regular" (representing conventional operation) and "inverted" (representing electrochemical stress conditions resulting from typical operating accidents) polarisation of the cathodic and anodic half-cells have been applied for 24 h each. The potential is first applied in the “regular” mode (i.e. cathodic -2V for the cathodic cell (a) and anodic +2V for the anodic one (b)) and then with the “inverted” polarisation (i.e. anodic +2V for the cathodic cell (a) and cathodic -2V for the anodic one (b)). During the electrochemical testing cycles in which the Fe interconnects are subject to anodic polarisation, they were found to develop both local (Figure 2-A) and global (Figure 2-B) thinning, resulting from the pitting corrosion mode and the current density distribution, respectively.

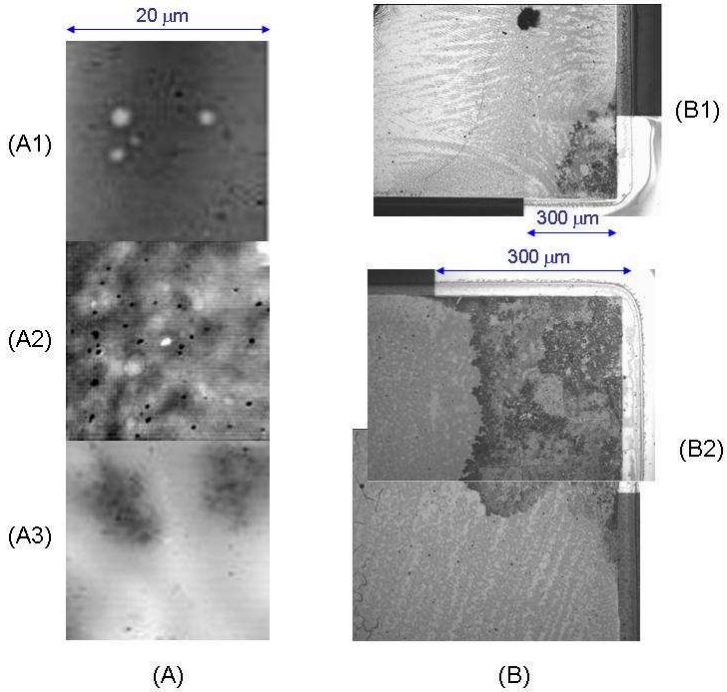

Figure 2 - STXM (A) and OM (B) micrographs of the corroded Fe electrodes of the nano-fuel-cell, showing thinning of the metal nanofilms on different scales. Image (A1), (A2) and (A3) were recorded at increasing distances from the metal/electrolyte edge.

Images (A1), (A2) and (A3) were recorded at increasing distances from the metal/electrolyte edge and bear a clear correlation with the long-scale thinning (lighter image implies higher X-ray transmitted intensity and hence lower thickness of the Fe film). (A1) highlights a few corrosion pits, (A2) shows the formation of relatively larger thinned areas, developing from the initial pits, in (A3) residual absorbing Fe island can be noticed on a light background. The Fe electrode of image (B1) was not directly connected to the potentiostat and it worked in a bipolar configuration between the Au cathode (not shown) and Fe anode (B2). In Figure 3, we report a selection of cracking patterns, developing into spirals. Micrograph A exhibits the edge of film dissolution front facing the electrolyte at the upper right corner of the image and a corrosion failure, leading to the formation of a hole in the Fe layer, surrounded by the lift-off and folding of the film at the bottom left corner. Panels B and C are magnifications of the spiral cracks shown in the central part of Panel A. Panels D-F show a representative collection of other spiral cracks found on the Fe nanofilm anode.

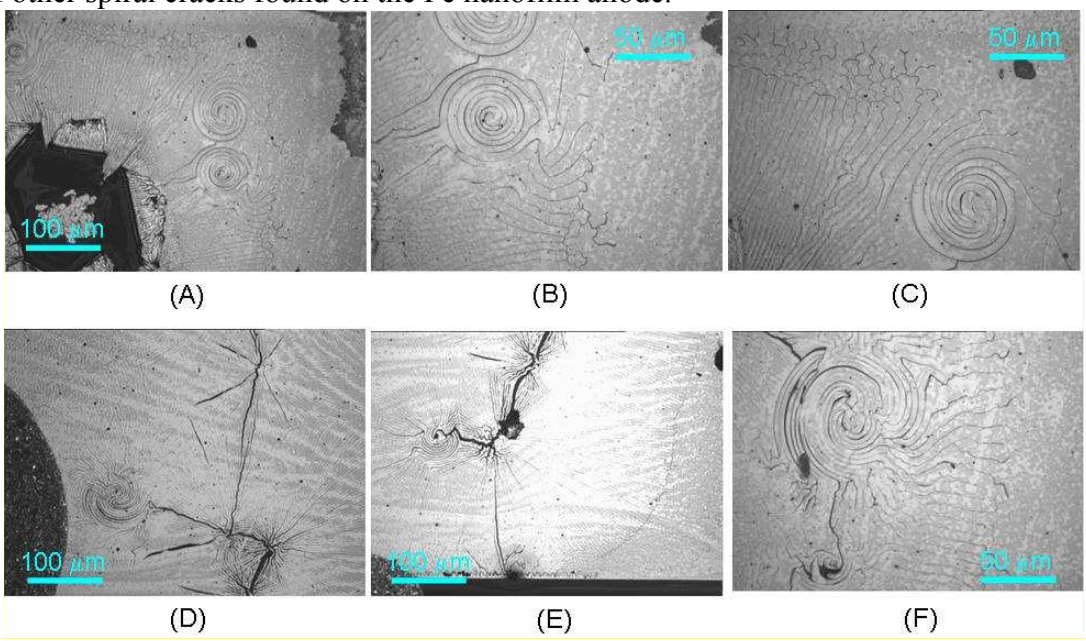

Figure 3 - Micrographs of the nano-fuel-cell Fe connectors, showing mechanical failures developing during electrochemical operation

Mechanical aspects related to the spiral cracks: a possibile generating mecchanism

The spiral cracks represent a fascinating subject of investigation within the realm of continuum mechanics. This class of fracture modes is found in different fields of engineering. Failure modes occurring in electronic devices at the metal-insulator interface can derive from the practice of forming electrical conduction paths in an insulating material by filling cylindrical holes with molten metal. This fabrication procedure results in a high residual stress field when the metal cools: owing to geometric constraints, cooling stresses are larger near the metal-insulator interface.

Stress relaxation thus tends to occur either by means of a de-bonding process or by the growth of cracks along paths which spiral away from the interface into the brittle material. In [14] spiral crack patterns occur in a completely different mechanical situation: thin layers of precipitates desiccating in contact with a substrate. This failure mode is found to arise naturally from a propagating stress front, induced by the fold-up of the fragments. Because of the humidity gradient across the thickness, the fragments gradually fold up and detach from the substrate, generating large tensile stresses in the radial direction, at the front of detachment and perpendicularly to it (Figures 4-A, panels (a) and (b)). The extent of the attached area thus shrinks as the ring-shaped front advances inward due to ongoing desiccation. When the stress at the front exceeds the local material strength, a crack is nucleated (Figure 4-A (b)). Since the nucleation is seldom symmetrical with respect to the boundaries, the crack tends to propagate along the front in one preferred direction, where more stresses can be released. In the absence of a further nucleation event, by the time the crack growth completes a cycle, the front has already advanced, forcing the crack to turn further inward, resulting eventually in a spiral crack (Figure 4-A (c)). Since the stresses on the top of the layer are mostly relieved by folding, they are concentrated at the layer-substrate interface. Therefore, the spiral runs like a tunnel, with a penetration into the layer thickness. The predominance of the spiral pattern indicates that crack propagation is favored over nucleation, otherwise more cylindrical concentric patterns would be observed.

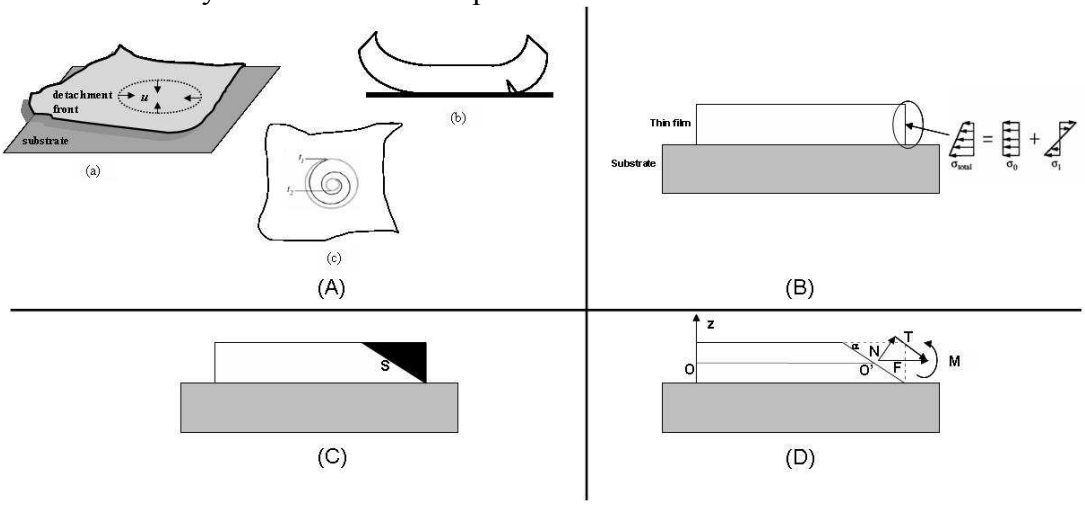

Figure 4 – (A) Spiral crack propagation mode in lifting films. (B) Schematic stress distribution in Si_3N_4-supported Fe films. (C) Schematic shape change of Fe film due to material loss caused by corrosion. (D) Simplified mechanical scheme of forces developing owing to material loss brought about by corrosion.

We conjecture that an explanation of the mechanism generating spiral cracks in nano-film Fe electrodes, supported on the chemically and mechanically stable Si_3N_4 substrate, can be based on these literature results. It is well known that the process employed for the fabrication of thin film electrodes - consisting in the evaporation of the desired amount of metal, that condenses on the substrate kept at room-temperature -, gives rise

to the formation of residual stresses [15, 16]. In Figure 4-B a typical schematic stress field distribution is represented in a section of the film. During the corrosion process, the Fe electrodes undergo space-dependent material losses, while the Au ones remain intact. Owing to the current density distribution prevailing in this system (see Figure 1), the corroding Fe electrodes become progressively thinner at the corner facing the polarised Au electrode. This loss of material has a mechanical impact, since the global equilibrium of the film subjected to an internal equilibrated stress field is perturbed. In Figure 4-C we show a schematic representation of the localisation of material loss distribution due to corrosion. From a mechanical standpoint, this loss of material results in an equivalent external load acting on the residual portion of film, due to the removal of a portion of the solid that was originally in equilibrium with the residual part. The relevant force balance is represented in Figure 4-D: the residual stress relieved by the loss of material results in a force F (N and T are the components normal and tangential at the plane of loss) and a bending momentum M, that are responsible for the related film deformation. If σ_0 and $\sigma_1(z)$ are the two components of residual stress (constant and varying with thickness z, respectively) evaluated with the method presented in [16], these forces will be: $N = A \cdot \sigma_0 \cdot \sin\alpha$ and $T = A \cdot \sigma_0 \cdot \cos\alpha$ and the momentum $M = b \cdot \sin\alpha \cdot \int_{-h/2}^{+h/2} \sigma_1(z) \cdot z \cdot dz$, where α is the angle of the plane of loss, A and b are the film cross-section area and width at the considered section S, h is the film thickness and the moment M is evaluated respect to the center O'. We note that the signs of F and M depend on the film and substrate materials as well as on the fabrication process: as a consequence, the films can crack in different ways depending on the values of F, M and the boundary conditions: from the literature, the relevant material combination and the geometry of interest are expected to yield compressive residual stresses [15, 17]. Thus, the stress field expected to develop on the basis of the simplified model presented above, is coherent with the scenarios proposed in the literature for the formation of spiral cracks [18, 19]. Of course, the real experimental situation we are faced with in our operating devices is much more complex, as well as time-dependent - since the electrochemical process gives rise to a time-dependent material loss, resulting in incresing values of F and M as time lapses –: these factors can be implemented a more accurate and datailed mechanoelectrochemical model along the lines schetched here, that allow to capture the key qualitative aspects of the observed cracking patterns.

CONCLUSIONS

In this work we report on peculiar mechanical failures occurring in nanometer-thick Fe electrode of fuel cells used for synchrotron-based in situ STXM studies. As a result of electrochemical corrosion during operation – leading to localised as well as global, spatially heterogeneous thinning of the Fe nanofilms –, complex crack patterns develop, including spiral ones. This special form of metal damaging is documented by STXM and optical microscopy of the damaged cells in the aggressive environment. The

formation of spiral cracks is justified with a simple mechanical model showing that the mechanical requirements recognised in the literature as necessary for the formation of spiral cracks are in fact met during the corrosion process. This paper contributes to the understanding of mechanical aspects of the failure of miniaturised devices for electrochemical generation of electrical power and offers insights for improved design in view of enhanced durability.

REFERENCES

[1] Bozzini, B. Gianoncelli, A. Kaulich, B. Kiskinova, M. Mele, C. Prasciolu, M. (2011) *PCCP* **13**, 7968-7974.
[2] Bozzini, B. Mele, C. Gianoncelli, A. Kaulich, B. Kiskinova, M. Prasciolu, M. (2011) *Microel. Eng.* **88**, 2456-2458.
[3] Gianoncelli, A. Kaulich, B. Kiskinova, M. Prasciolu, M. D.Urzo, L. Bozzini, B. (2010) *Micron* **42**, 342-347.
[4] Bozzini, B. Gianoncelli, A. Kaulich, B. Kiskinova, M. Prasciolu, M. Sgura, I. (2010) *ChemSusChem* **3** 846-850.
[5] Bozzini, B. D'Urzo, L. Gianoncelli, A. Kaulich, B. Prasciolu, M. Sgura, I., Tondo, E. and Kiskinova, M. (2009) *J. Phys. Chem. C* **113**, 9783-9787.
[6] Bozzini, B. D'Urzo, L. Gianoncelli, A. Kaulich, B. Kiskinova, M. Prasciolu, M. Tadjeddine, A. (2008) *Electrochem. Comm.* **10**, 1680-1683.
[7] Curtin, D.E. Lousenberg, R.D. Henry, T.J. Tangeman, P.C. Tisack, M.E. (2004) *J. Power Sources* **131**, 41-48.
[8] x Schmittinger, M.E. Vahidi, A. (2008) *J. Power Sources* **180**, 1-14.
[9] Marcus, P. Maurice, V. Strehblow, H.-H. (2008) *Corros. Sci.* **50**, 2698-2704.
[10] Show, Y. Takahashi, K. (2009) *J. Power Sources* **190**, 322-325.
[11] Bozzini, B. Tondo, E. Prasciolu, M. Amati, M. Kazemian Abyaneh, M. Gregoratti, L. and Kiskinova, M. (2011) *ChemSusChem* **4**, 1099-1103.
[12 Lux, K.W. Rodriguez, K.J. (2006) *Nanoletters* **6**, 288-295.
[13] Mele, C. Bozzini, B. (2010) *J. Power Sources* **195**, 3590-3596.
[14] Néda, Z. Leung, K.-T. Jozsa, L. Ravasz, M. (2002) *Phys. Rev. Lett.* **88**, 095502.
[15] Mebarkia, M. Layadia, A. Guittoumb, A. Benabbasc, A. Gheboulia, B. Saadb, M. Mennid, N. (2011) *Appl. Surf. Sci.* **257**, 7025–7029.
[16] Fang, W. Wickert, J. A. (1996) *J. Micromech. Microeng.* **6**, 301–309.
[17] Chason, E. Sheldon, B.W. Freund, L. B.J. Floro, A. and Hearne, S. J. (2002) *Phys. Rev. Lett.* **88**, 156103.
[18] Wang, J.-X. Huang, Z.-P. Duan, H.-L. Yu, S.-W. Feng, X.-Q. Wang, G.-F. Zhang, W.-X. Wang, T.-J. (2011) *Acta Mechanica Solida Sinica*, **24**, 52-82.
[19] Lu, P. Le, L.H. Lee, H.P. Lu, C. (2006) *Int. J. Solids and Structures* **43**, 4631-4647.